Solar Energy Materials & Solar Cells 97 (2012) 43–49

Contents lists available at SciVerse ScienceDirect

Solar Energy Materials & Solar Cells

journal homepage: www.elsevier.com/locate/solmat

Roll-to-roll processed polymer tandem solar cells partially processed from water

Thue T. Larsen-Olsen, Thomas R. Andersen, Birgitta Andreasen, Arvid P.L. Böttiger, Eva Bundgaard, Kion Norrman, Jens W. Andreasen, Mikkel Jørgensen, Frederik C. Krebs *

Risø National Laboratory for Sustainable Energy, Technical University of Denmark, Frederiksborgvej 399, DK-4000 Roskilde, Denmark

ARTICLE INFO

Available online 21 September 2011

Keywords:
Roll-to-roll processing
Tandem solar cells
Polymer solar cells
Printing and coating
Aqueous processing

ABSTRACT

Large area polymer tandem solar cells completely processed using roll-to-roll (R2R) coating and printing techniques are demonstrated. A stable tandem structure was achieved by the use of orthogonal ink solvents for the coating of all layers, including both active layers. Processing solvents included water, alcohols and chlorobenzene. Open-circuit voltages close to the expected sum of sub cell voltages were achieved, while the overall efficiency of the tandem cells was found to be limited by the low yielding back cell, which was processed from water based ink. Many of the challenges associated with upscaling the multilayer tandem cells were identified giving valuable information for future experiments and development.

1. Introduction

The ultimate efficiency of polymer solar cells is inherently limited by the narrow absorption bands of the chromophores that constitute the photoactive layer of the solar cells. One obvious route to circumvent this is to stack several junctions having complementary absorption bands, thus increasing the spectral overlap of the solar cell and the terrestrial solar spectrum. The benefits of the tandem architecture over single junction cells have been thoroughly studied and reviewed [1–4], and within reasonable assumptions it has been found that a tandem architecture can increase the ultimate efficiency of polymer solar cells with 20–50%, where the highest increase is seen in the case where the single junction cells perform under their ultimate potential [1,2].

The most advantageous approach to polymer solar cell fabrication, with respect to application as an energy technology, is to allow for fast processing of all layers relying on as few coating/printing methods as possible using roll-to-roll (R2R) processing. With regards to tandem polymer solar cells the most obvious device is an all solution processed monolithic tandem cell where the sub cells are connected in series rather than parallel. This naturally presents some challenges in multilayer coating where the typical number of layers required in a tandem cell is around 6–8. All these layers (some of them very thin) have to be coated on top of each other without having subsequent coating steps adversely affecting already coated layers. The traditional laboratory approach to building up the stack is thus not expected to be easily scalable since it often employs vacuum deposition of many of the layers and a rational choice in the order of application. With the boundary condition that all layers have to be processed in air without vacuum, using only solution based printing and coating techniques, it becomes very challenging to realize functional tandem structures. So far only one report has documented vacuum free solution processing of all layers, including the printed metal back electrode [5], while large stacks by solution processing (and vacuum deposited back electrodes) have been reported [6]. Most tandem solar cell reports today employ one or more vacuum coating steps.

In this report we demonstrate R2R processing of tandem polymer solar cells on flexible substrates and show that there are many challenges associated not only with solution processing of entire tandem solar cell stacks, but also with the transfer from laboratory scale batch processing on rigid substrates to a full R2R only process on flexible films.

2. Experimental section

2.1. Materials

Poly-3-hexylthiophene (P3HT) was commercially available and had an M_n of ~20000 Da and an M_w ~40000 Da. Phenyl-C_{61}-butyric acid methyl ester (PC[60]BM) had a purity of 99%. Poly-[thiophene-2,5-diyl-*alt*-(2,3-bis(3-octyloxyphenyl)quinoxaline-5,8-diyl] (TQ-1) was synthesized according to the method described in the literature [7] and had an M_n of ~29000 Da and an M_w ~89000 Da.

The ink used for the front bulk heterojunction (BHJ) active layer comprised PC[60]BM as the acceptor material (18 mg mL^{-1}) and

* Corresponding author. Tel.: +45 46 77 47 99.
E-mail address: frkr@risoe.dtu.dk (F.C. Krebs).

0927-0248/$ - see front matter © 2011 Elsevier B.V. All rights reserved.
doi:10.1016/j.solmat.2011.08.025

P3HT as the donor polymer (22 mg mL^{-1}) dissolved in chlorobenzene. For the back BHJ active layer an aqueous ink [8] comprising an aqueous dispersion of nanoparticles consisting of the low band gap polymer TQ-1 (Fig. 1) and PC[60]BM prepared as described earlier [8]. An aqueous precursor solution for the zinc oxide (ZnO) used as electron transporting layer (ETL) was prepared as described earlier [9] and comprised $Zn(OAc)_2$ $2H_2O$ (100 mg mL^{-1}), $Al(OH)(OAc)_2$ (2 mg mL^{-1}) and FSO-100 (2 mg mL^{-1}) in water. Vanadium(V)oxide (V_2O_5) employed as hole transporting layer (HTL) was prepared by diluting a base solution of vanadium(V)-oxiisopropoxide with isopropanol to a concentration of 25 mg mL^{-1}, following recommendations of earlier studies [10,11]. Poly(3,4-ethylenedioxythiophene) poly(styrenesulfonate) (PEDOT:PSS) was based on Orgacon EL-P 5010 from Agfa diluted 2:1 (w:w) with isopropanol. The printable silver back electrode was PV410 from Dupont. The substrate was a 130 micron PET substrate with a patterned ITO layer (nominally 60 Ω $square^{-1}$).

2.2. Slot-die coating

The bottom electron contact was prepared directly on the PET/ITO substrate, prepared and cleaned as described earlier [12]. The zinc oxide precursor solution was microfiltered immediately prior to use (filter pore size of 0.45 μm) and then slot-die coated at a speed of 2 m min^{-1} with a wet thickness of 4.9 μm. After the initial drying of the precursor film it was converted into an insoluble film by passage through an oven at a temperature of 140 °C with a speed of 0.2 m min^{-1} (oven length=4 m). This gave an insoluble doped zinc oxide film with a thickness of 25 ± 5 nm. The P3HT:PC[60]BM ink described above was microfiltered and slot die-coated with at a web speed of 1.6 m min^{-1} and a wet thickness of 11.2 μm. The film was dried by passage through an oven (2 m) at 140 °C. The recombination layer comprised a V_2O_5/ZnO stack that was slot-die coated in two steps. The V_2O_5 layer was slot-die coated directly on top of the dried P3HT:PC[60]BM layer, with a web speed of 2 ml min^{-1} and a wet thickness of 8 μm. The film was dried by passage through an oven (2 m) at 140 °C. The second zinc oxide layer was prepared exactly as the first (anode) layer, directly on the V_2O_5 layer. The back cell was prepared by slot-die coating an aqueous TQ-1:PC[60]BM nanoparticle dispersion (Fig. 2) at a web speed of 0.2 m min^{-1} and a wet thickness of 30 μm. The wet film was dried at 140 °C (oven length=2 m) as described earlier [8]. The back electrode was prepared by applying PEDOT:PSS by slot-die coating at a speed of 0.2 m min^{-1} with drying at 140 °C (oven length=2 m). It was found unnecessary to wet the film surface prior to coating the PEDOT:PSS and this might be due to the beneficial interaction between the fluorosurfactants in the aqueous nanoparticle dispersion and in the PEDOT:PSS. Finally, the device was completed by R2R screen printing a silver grid electrode and drying at 140 °C. The devices were encapsulated using R2R lamination of a simple food packaging barrier with a pressure sensitive adhesive onto both sides of the foil [12b].

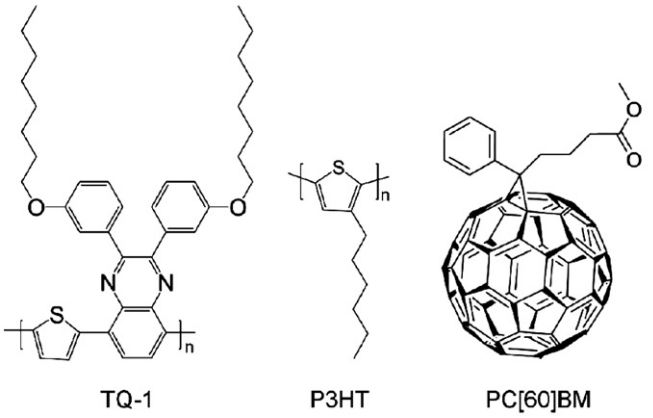

Fig. 1. Structure of poly-[thiophene-2,5-diyl-*alt*-(2,3-bis(3-octyloxyphenyl)quinoxaline-5,8-diyl] (TQ-1), poly-3-hexylthiophene (P3HT), and phenyl-C_{61}-butyric acid methyl ester (PC[60]BM).

2.3. TOF-SIMS depth profiling analysis

Time-of-flight secondary ion mass spectrometry (TOF-SIMS) was employed to perform a depth profiling analysis. The experiments were conducted using a TOF-SIMS IV (ION-TOF GmbH, Münster, Germany). 25-ns pulses of 25-keV Bi^+ (primary ions) were bunched to form ion packets with a nominal temporal extent of <0.9 ns at a repetition rate of 10 kHz yielding a target current of 1 pA. These primary ion conditions were used to obtain depth profiles in both negative and positive ion mode. Depth profiling was performed using an analysis area of 100×100 μm^2

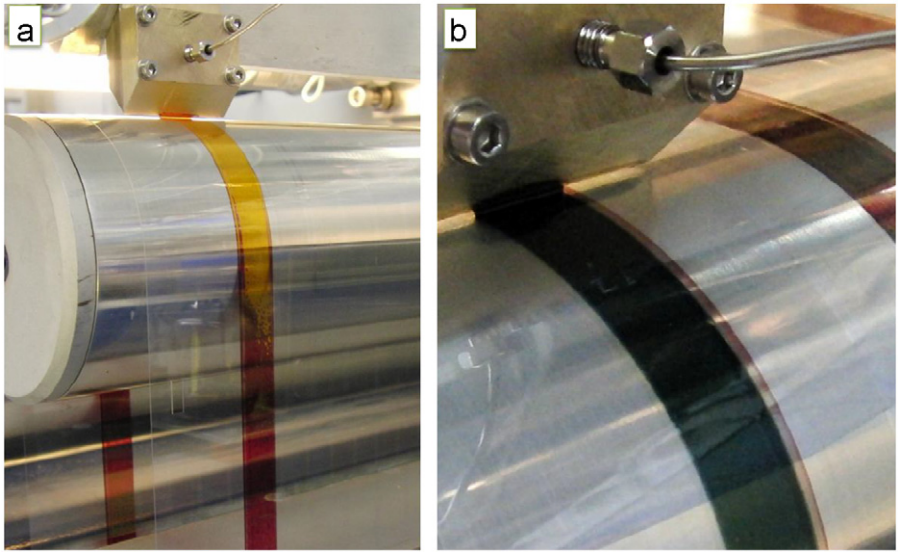

Fig. 2. Photographs of the actual R2R coating experiment in progress. (a) Coating of the front BHJ material (the drying process of the film is visible). (b) Coating of the back BHJ material.

and a sputter area of $300 \times 300\ \mu m^2$. 30 nA of 3-keV Xe^+ were used as sputter ions. Electron bombardment (20 eV) was used to minimize charge build-up at the surface. Desorbed secondary ions were accelerated to 2 keV, mass analyzed in the flight tube, and post-accelerated to 10 keV before detection.

2.4. J–V characterization

The final devices were put under simulated sunlight at $1000\ W\ m^{-2}$, $85 \pm 5\ ^\circ C$, $40 \pm 10\%$ relative humidity (rh) (AM1.5G). *J–V* curves were recorded by sweeping from -1 V to $+1$ V in steps of 20 mV and a rate of $0.1\ V\ s^{-1}$ to ensure that no dynamic effects resulted in over/under estimation of J_{sc} and V_{oc}. The time evolution of the photovoltaic performance was recorded by continuously illuminating the device under the above conditions while recording complete IV data every one minute according to ISOS-L-1 [13].

3. Results and discussion

3.1. The tandem cell

This study describes the transfer of a laboratory scale tandem solar cell process on rigid glass substrates to a R2R process on flexible plastic substrates. The laboratory process was described previously [11] and was developed with an aim of being compatible with R2R processing. The tandem solar cell structure comprised a multilayer stack with the composition PET/ITO/ZnO/front-BHJ/V_2O_5/ZnO/back-BHJ/PEDOT:PSS/Ag, where PET is poly(ethylene terephthalate) (substrate), ITO is indium tin oxide (transparent front electrode), ZnO is the electron transport layer, front-BHJ is the front bulk heterojunction consisting of P3HT:PC[60]BM (active layer 1), V_2O_5/ZnO is the recombination layer, back-BHJ consists of TQ-1:PC[60]BM (active layer 2), PEDOT:PSS is the hole transport layer, and Ag is the back electrode. Illustrative photographs of the coating process are shown in Fig. 2.

The first attempts resulted in very poorly performing devices typically showing open-circuit voltages around what is expected for single junction devices. Optical inspection of the completed devices revealed the possible origin of this malfunction to be cracks in the V_2O_5 part of the recombination layer (Fig. 3). It was found that these cracks form at some point during the processing of the V_2O_5 layer, possibly due to the heat treatment and/or bending of the substrate as it passes through the R2R equipment. As is also hinted in Fig. 3 these cracks persist after processing of the ZnO layer thus rendering the recombination layer penetrable to the solute of the back BHJ as this is coated. This would most likely solubilize the front BHJ and thus seriously compromise the integrity of the serial connection of the two sub cells. This situation is schematically described in Fig. 4a. Such a short-circuiting of the recombination layer would make the two active layers effectively function as one poorly performing active layer, in turn, explaining the single junction-like low open-circuit voltage observed for these devices.

However, it was possible to work around this issue by utilizing an aqueous ink for the processing of the back BHJ using a method recently described by Andersen et al. [8]. This presented a unique opportunity for orthogonal processing since water cannot solubilize the front BHJ. From the photomicrographs shown in Fig. 4 it is evident that the back cell looks less affected by the cracks in the recombination layer when water based processing is employed (Fig. 4b compared to Fig. 4a).

3.2. TOF-SIMS depth profiling analysis

TOF-SIMS depth profiling analysis was employed in both negative and positive ion mode in order to document the layer stack order. The encapsulation film is too thick for a depth profiling analysis, so it was necessary to delaminate the tandem solar cell. TOF-SIMS mass spectra of the exposed surfaces revealed that delamination took place at the PEDOT:PSS/back BHJ interface.

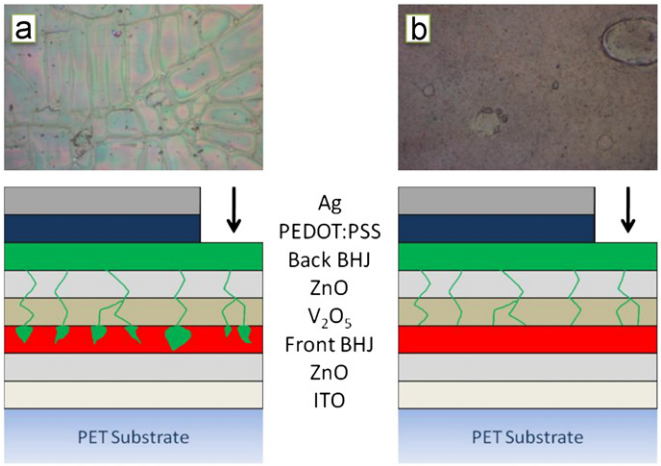

Fig. 4. Schematics of the tandem solar cell under study and photomicrographs ($230 \times 150\ \mu m^2$) obtained at the indicated positions (black arrows), which illustrates the proposed consequence of the observed cracks in the recombination layer when using (a) a non-orthogonal solvent (chloroform) and (b) an orthogonal solvent (water), for the processing of the back BHJ.

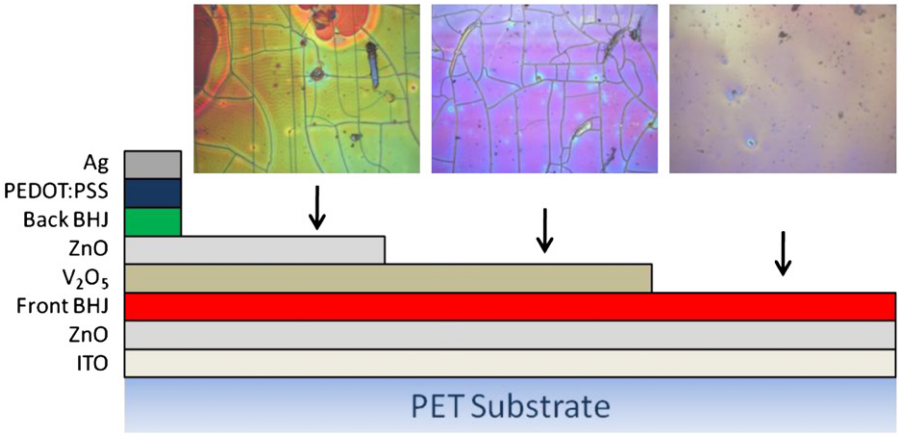

Fig. 3. Schematic of the tandem solar cell under study and photomicrographs ($260 \times 195\ \mu m^2$) revealing cracks in the V_2O_5 layer, which persist through the ZnO layer.

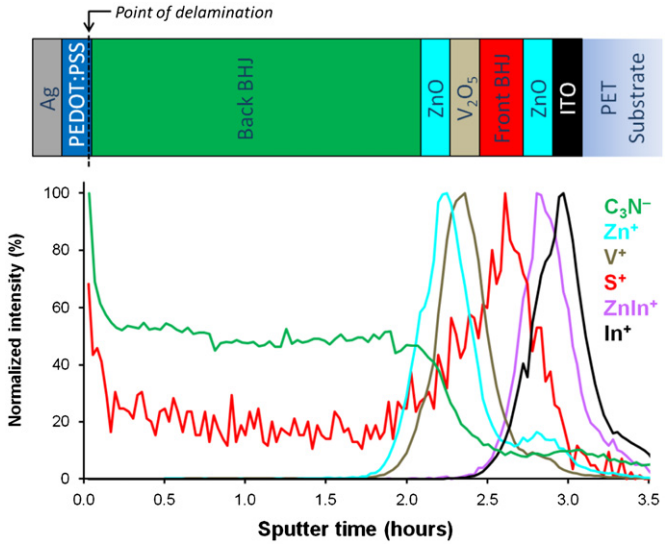

Fig. 5. TOF-SIMS depth profiles through the delaminated tandem solar cell. C_3N^- is a marker for the back BHJ obtained from a depth profile run in negative mode, Zn^+ is a marker for the ZnO, V^+ is a marker V_2O_5, S^+ is a marker for both front and back BHJ, and $ZnIn^+$ (formed during the ionization step of the analysis) is a marker for the front ZnO and In^+ is a marker for ITO.

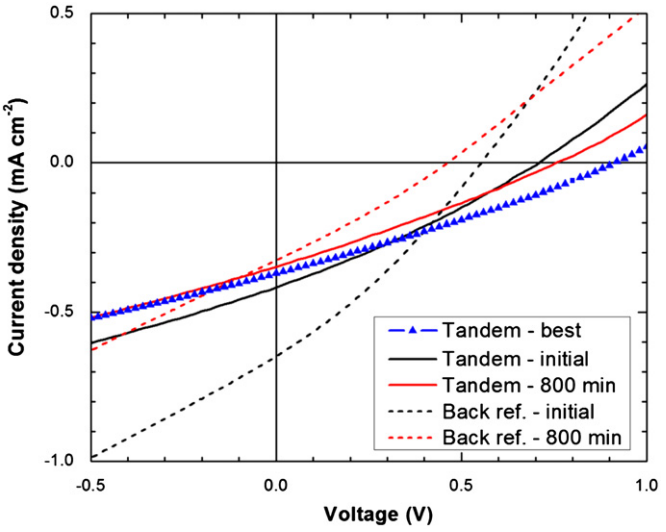

Fig. 6. *J–V* characteristics (AM1.5G 1000 W m^{-2}) for the best performing tandem cells. Also shown is a more average cell, before (initial) and after (800 min) photo-annealing.

Fig. 5 shows the results of the depth profile analysis. Various factors complicated the analysis, such as interface roughness, which is well known phenomenon in R2R processing (e.g. compared to spin coating). Furthermore, depth profiling in soft materials is associated with an inferior depth resolution (under the given sputter conditions), compared to hard materials (e.g. metals). These conditions constitute a challenge especially when it comes to performing depth profiling on very thin layers such as the ZnO (~25 nm) and V_2O_5 (~15 nm) layers present in this device. However, as is evident from Fig. 5 it was quite possible, in spite of the conditions, to document the multilayer stack composition in the tandem solar cell device. Residual PEDOT:PSS was present in the PEDOT:PSS/back BHJ interface after the delamination process presumably due to a small degree of interlayer mixing that resulted in presumably a matrix effect, which is observed as initially elevated signals from the back BHJ material (i.e. at the beginning of the sputter time window). During the ionization process the Zn^+ signal is discriminated due to the formation of the $ZnIn^+$ cluster ion caused by the close vicinity of the ITO (i.e. an ionization phenomenon). Finally, a significantly long sputter time window is observed for the back BHJ compared to the front BHJ, which suggests that the back BHJ is significantly thicker (assuming similar sputter rates) than the front BHJ consistent with an expected layer thickness of ~600 nm [8] for the back BHJ as compared to the thickness of the front BHJ ~200 nm.

3.3. Electrical characterization

J–V characteristics for the best performing tandem device are shown in Fig. 6, (blue triangles) together with representative *J–V* curves for both tandem and back cell reference devices with and without photo-annealing (800 min). The key photovoltaic parameters are summarized in Table 1, while the dynamic evolutions of the short circuit current (I_{sc}) and open-circuit voltage (V_{oc}) are shown in Fig. 7. By summing the V_{oc} values from the sub cell reference devices (Table 1) it is possible to estimate that the perfect tandem device would have an open-circuit voltage close to 1 V. As is clear from the presented data in Table 1, the actual tandem devices gave, at best, a V_{oc} around 0.9 V while V_{oc} values around 0.75 V were readily measured, hence between 0.1 and 0.25 V less than the expected ideal value.

Table 1
Summary of the *J–V* characterization.

Cell	PCE (%)	J_{sc} (mA cm^{-2})	V_{oc} (V)	FF (%)
Tandem [a]				
(Initial)	0.09	−0.42	0.71	28.8
(800 min)	0.07	−0.35	0.76	27.5
(Best)	0.10	−0.37	0.91	28.2
Back cell [a]				
(Initial)	0.11	−0.65	0.55	30.2
(800 min)	0.04	−0.33	0.46	27.7
Front cell (Ref. [11])	1.32	−7.17	0.50	36.9

[a] Cell active area of 4 cm^2.

Various loss mechanisms can influence the tandem voltage, of which most are related to the nature of the sub cell interconnection, i.e. the recombination layer. In this case it is highly probable that the before mentioned observed defects (Fig. 3) are likely to have a negative influence on V_{oc} if the mechanism schematically shown in Fig. 4b is considered, i.e. shunts across the recombination layer would lower the tandem V_{oc}. Furthermore, the results show that the front and back reference cells both exhibit a decreasing V_{oc} during the dynamic evolution *J–V* experiment as observed in Fig. 7 and S7 (see e-component). For the tandem devices the trend is opposite, i.e. increasing V_{oc} over time. Both reference cells display saturation at around 0.45 V, which fits well with the peak value of the best tandem cell.

It appears that the sub cell interconnection improves over time, possibly due to burning of shunts across the recombination layer, originally formed as a consequence of the defects. With respect to the I_{sc} it is noticeable that the tandem device and the back cell reference device have rather similar I_{sc} values. This should be compared to the front cell I_{sc}, which is a factor of 10 to 20 times larger. Thus the tandem device is severely current limited by the poor performing back cell.

This significant current mismatch is likely to influence the current–voltage characteristics of the tandem cell. Hadipour et al. [14] found that the excess current will cause the surplus of free holes to pile up at the middle electrode (recombination layer), which will result in a lowering of the effective internal field in the

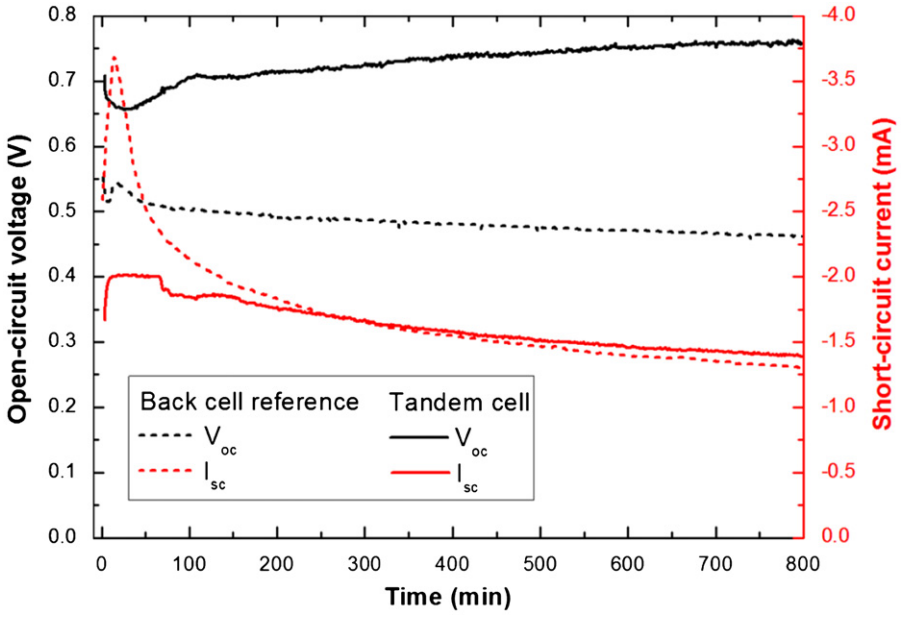

Fig. 7. Time evolution of the open-circuit voltage and short-circuit current during the 800 min of photo-annealing (AM1.5G 1000 W m^{-2}) of the tandem cell, and a corresponding single junction reference cell mimicking the current-limiting back cell.

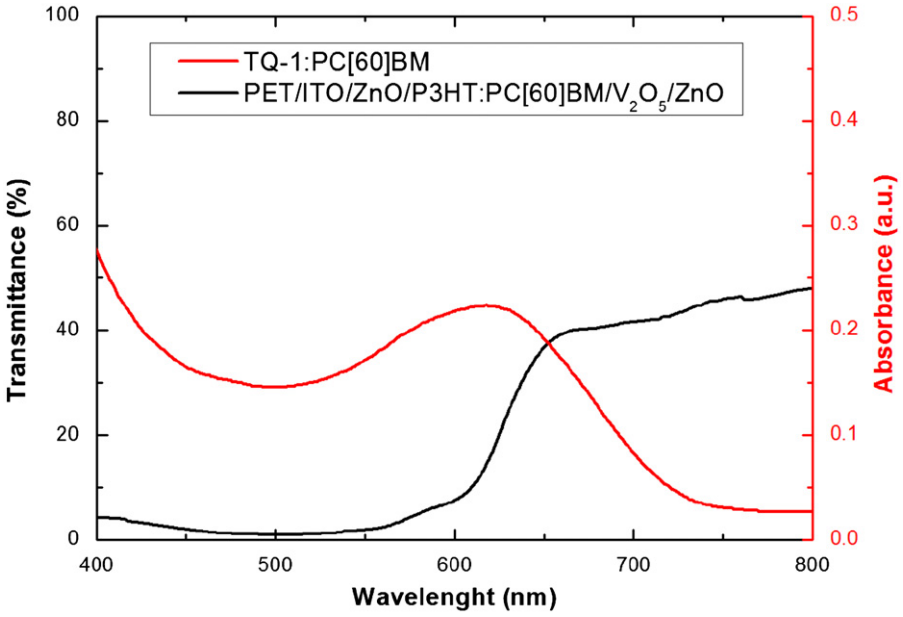

Fig. 8. Transmittance of the front cell and the recombination layer relative to the absorbance of the back cell active layer.

front sub cell, while for the back sub cell the opposite will be the case and the internal field will increase.

Hence the sub cell currents will equilibrate at some intermediate value, resulting in a higher I_{sc} value for the tandem device compared to the expected current of the limiting sub cell reference device. How the tandem current equilibrates is very much dependent on the slope of the *J–V* curves of the sub cells around short-circuit as well as the degree of current mismatch, as recently pointed out by Braun et al. [15] for the case of an inorganic tandem cell. This can be easily understood, e.g. in the case of the current limiting sub cell; as the reverse biasing caused by the current mismatch will only result in a significant increase in current if the *J–V* curve of the sub cell has a non zero slope in reverse bias, which is the case for the cells under study here. Furthermore, according to Fig. 8 the tandem back cell will suffer from an obvious poor spectral matching with the front cell transmission spectrum, and thus receive a significantly lower photon flux than the reference cell. From this, a significant lowering of the back cell current would be expected. However, as the *J–V* data shows that the I_{sc} of the tandem is not lower but rather comparable to that of the current limiting back cell reference device this would in fact imply a combination of the spectral mismatch and the increased quantum efficiency of the tandem back cell due to current mismatch (the effect described in Refs. [14 and 15]). To support this, we construct the ideal tandem curve from the two reference sub cells by summing voltages at equal currents, as described in Ref. [14]. We take into account the spectral mismatch by a mismatch factor *S*, which is simply multiplied with the current of the back cell reference. These can be seen in Fig. 9, for the case of $S=1$ and $S=0.5$, together with the

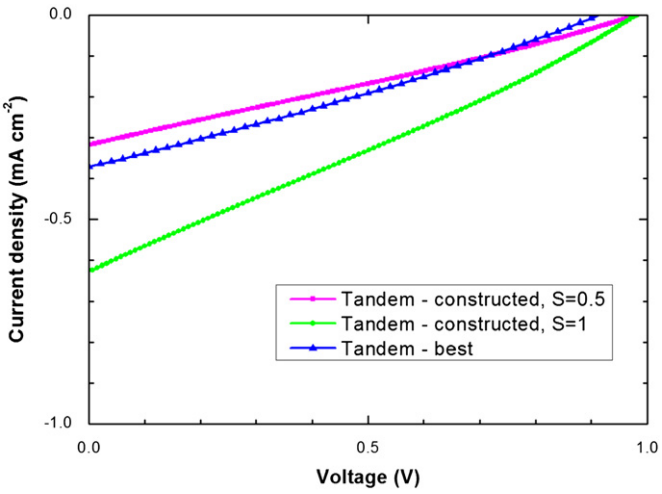

Fig. 9. Constructed tandem J–V characteristics with spectral mismatching ($S=0.5$) and without ($S=1$), compared with the best measured tandem device.

best tandem curve. As can be seen, it is likely that severe spectral mismatching is the cause of the low short-circuit current of the tandem cell, while the discrepancy between the model and the measurement can be explained by the somewhat crude model, such as negligence of V_{oc} dependence on light intensity [16], and the assumption of a perfect ohmic connection between the sub cells, e.g. a perfect recombination layer.

3.4. Future developments

The tandem approach within polymer photovoltaics has so far been utilized in an attempt to maximize efficiency, i.e. without constraints on materials and fabrication methods. The present work, however, demonstrates the fragility of the tandem device approach from a solution processing point of view, and in doing so, stresses the importance of having certain constraints in mind when assessing a given set of materials and processing methods. In this regard especially the recombination layer presents an all-determining weak-point of the tandem cell; a perfect recombination layer would be insoluble and solvent impenetrable, being either a pn-junction preferably a highly doped tunnel junction or alternatively having metal like characteristics. This has so far been achieved only for small area devices using rigid substrates [6,11,17–21]. Lee et al. [22] successfully demonstrated a small area tandem device on a flexible substrate but using vacuum deposition. However, as for upscaling of the fabrication, it is the view of the authors that a stable and highly reliable solution process for polymer tandem solar cells can only be ensured by a completely orthogonalized process in which none of the processing steps can seriously harm any of the previously processed layers. This has to do with the inherently rough nature of a high throughput R2R process, during which cracks and small coating imperfections would act as solvent paths leading to partial dissolution of underlying layers. The aqueous emulsion approach utilized in this work is one possible solution presenting both a stable and possibly environmentally friendly fabrication process. At the same time it allows for the use of the large amount of existing polymers. However, the success of this technique of course depends on whether significantly better device performance can be achieved. Another foreseeable solution would be a process where the layers by some in-line post process are rendered insoluble, for instance using thermal- or light-induced thermocleavage of the solubilizing groups as demonstrated earlier [5,23,24]. This would be very desirable as it ensures free choice of solvent for the subsequent layers, and also removes constraints on the recombination layer in terms of materials and layer thicknesses, thus opening for a wider range of tweakable parameters.

4. Conclusions

We have successfully demonstrated large area flexible polymer tandem solar cells with all layers processed entirely from solution, and partially from water. The multilayer stack on flexible PET substrate comprised a cathode of ITO/ZnO, a recombination layer of V_2O_5/ZnO, and a PEDOT:PSS/Ag (printed) anode. The two serially connected BHJs was comprised of a P3HT:PC[60]BM front cell processed from chlorobenzene and a back cell processed from an aqueous dispersion of poly[2,3-bis-(3-octyl oxyphenyl)-quinoxaline-5,8-diyl-alt-thiophene-2,5-diyl]:PC[60]BM nanoparticles. The composition and integrity of the multilayer stack was confirmed by TOF-SIMS depth profiling. The V_{oc} of the best tandem device was 0.9 V, while both the corresponding single junction reference devices had a V_{oc} around 0.5 V. This confirms a serial connection of the sub cells while the observed voltage losses are ascribed to visible defects in the recombination layer and a non-ohmic connection of the two sub cells.

Acknowledgment

This work was supported by the Danish National Research Foundation. We gratefully acknowledge Lasse Gorm Jensen for creating graphical illustrations and Jon E. Carlé and Martin Helgesen for preparing polymer materials.

Appendix A. Supplementary materials

Supplementary data associated with this article can be found in the online version at doi:10.1016/j.solmat.2011.08.025.

Details of GIWAXS measurements and time evolution for the back reference cell.

References

[1] T. Ameri, G. Dennler, C. Lungenschmied, C.J. Brabec, Organic tandem solar cells: a review, Energy & Environmental Science 2 (2009) 347–363.
[2] G. Dennler, M.C. Scharber, T. Ameri, P. Denk, K. Forberich, C. Waldauf, C.J. Brabec, Design rules for donors in bulk-heterojunction tandem solar cells. Towards 15% energy-conversion efficiency, Advanced Materials 20 (2008) 579–583.
[3] J.D. Kotlarski, P.W.M. Blom, Ultimate performance of polymer: fullerene bulk heterojunction tandem solar cells, Applied Physics Letters 98 (2011) 053301.
[4] Y.M. Nam, J. Huh, W.H. Jo, A computational study on optimal design for organic tandem solar cells, Solar Energy Materials and Solar Cells 95 (2011) 1095–1101.
[5] O. Hagemann, M. Bjerring, N.C. Nielsen, F.C. Krebs, All solution processed tandem polymer solar cells based on thermocleavable materials, Solar Energy Materials and Solar Cells 92 (2008) 1327–1335.
[6] J. Gilot, M.M. Wienk, R.A.J. Janssen, Double and triple junction polymer solar cells processed from solution, Applied Physics Letters 90 (2007) 143512.
[7] E. Wang, L. Hou, Z. Wang, S. Hellström, F. Zhang, O. Inganäs, M.R. Andersson, An easily synthesized blue polymer for high-performance polymer solar cells, Advanced Materials 22 (2010) 5240–5244.
[8] T.R. Andersen, T.T. Larsen-Olsen, B. Andreasen, A.P.L. Böttiger, J.E. Carle′, M. Helgesen, E. Bundgaard, K. Norrman, J.W. Andreasen, M. Jørgensen, F.C. Krebs, Aqueous processing of low-band-gap polymer solar cells using roll-to-roll methods, ACS Nano 5 (2011) 4188–4196.
[9] R. Søndergaard, M. Helgesen, M. Jørgensen, F.C. Krebs, Fabrication of polymer solar cells using aqueous processing for all layers including the metal back electrode, Advanced Energy Materials 1 (2011) 68–71.
[10] N. Espinosa, H.F. Dam, D.M. Tanenbaum, J.W. Andreasen, M. Jørgensen, F.C. Krebs, Roll-to-roll processing of inverted polymer solar cells using hydrated vanadium(V)oxide as a PEDOT:PSS replacement, Materials 4 (2011) 169–182.

[11] T.T. Larsen-Olsen, E. Bundgaard, K.O. Sylvester-Hvid, F.C. Krebs, A solution process for inverted tandem solar cells, Organic Electronics 12 (2011) 364–371.
[12] a) F.C. Krebs, T. Tromholt, M. Jørgensen, Upscaling of polymer solar cell fabrication using full roll-to-roll processing, Nanoscale 2 (2010) 873–886;
b) J. Alstrup, M. Jørgensen, A.J. Medford, F.C. Krebs, Ultra fast and parsimonious materials screening for polymer solar cells using differentially pumped slot-die coating, ACS Applied Materials & Interfaces 2 (2010) 2819–2827.
[13] M.O. Reese, S.A. Gevorgyan, M. Jørgensen, E. Bundgaard, S.R. Kurtz, D.S. Ginley, D.C. Olson, M.T. Lloyd, P. Morvillo, E.A. Katz, A. Elschner, O. Haillant, T.R. Currier, V. Shrotriya, M. Hermenau, M. Riede, K.R. Kirov, G. Trimmel, T. Rath, O. Inganäs, F. Zhang, M. Andersson, K. Tvingstedt, M. Lira-Cantu, D. Laird, C. McGuiness, S. Gowrisanker, M. Pannone, M. Xiao, J. Hauch, R. Steim, D.M. DeLongchamp, R. Rösch, H. Hoppe, N. Espinosa, A. Urbina, G. Yaman-Uzunoglu, J.-B. Bonekamp, A.J.J.M. van Breemen, C. Girotto, E. Voroshazi, F.C. Krebs, Consensus stability testing protocols for organic photovoltaic materials and devices, Solar Energy Materials and Solar Cells 95 (2011) 1253–1267.
[14] A. Hadipour, B. de Boer, P.W.M. Blom, Device operation of organic tandem solar cells, Organic Electronics 9 (2008) 617–624.
[15] A. Braun, N. Szabo´, K. Schwarzburg, T. Hannappel, E. Katz, J.M. Gordon, Current-limiting behavior in multijunction solar cells, Applied Physics Letters 98 (2011) 223506.
[16] T. Tromholt, E. Katz, B. Hirsch, A. Vossier, F.C. Krebs, Effects of concentrated sunlight on organic photovoltaics, Applied Physics Letters 96 (2010) 073501.
[17] A. Hadipour, B. de Boer, J. Wildeman, F.B. Kooistra, J.C. Hummelen, M.G.R. Turbiez, M.M. Wienk, R.A.J. Janssen, P.W.M. Blom, Solution-processed organic tandem solar cells, Advanced Functional Materials 16 (2006) 1897–1903.
[18] J.Y. Kim, K. Lee, N.E. Coates, D. Moses, T.–Q. Nguyen, M. Dante, A.J. Heeger, Efficient tandem polymer solar cells fabricated by all-solution processing, Science 317 (2007) 222–225.
[19] S. Sista, M.–H. Park, Z. Hong, Y. Wu, J. Hou, W.L. Kwan, G. Li, Y. Yang, Highly efficient tandem polymer photovoltaic cells, Advanced materials 22 (2010) 380–383.
[20] D.J.D. Moet, P. de Bruyn, P.W.M. Blom, High work function transparent middle electrode for organic tandem solar cells, Applied Physics Letters 96 (2010) 153504.
[21] C.–H. Chou, W.L. Kwan, Z. Hong, L.–M. Chen, Y. Yang, A. Metal-Oxide, Interconnection layer for polymer tandem solar cells with an inverted architecture, Advanced Materials 23 (2011) 1282–1286.
[22] B.J. Lee, H.J. Kim, W. -ik Jeong, J.–J. Kim, A transparent conducting oxide as an efficient middle electrode for flexible organic tandem solar cells, Solar Energy Materials and Solar Cells 94 (2010) 542–546.
[23] T. Tromholt, S.A. Gevorgyan, M. Jørgensen, F.C. Krebs, K.O. Sylvester-Hvid, Thermocleavable materials for polymer solar cells with high open circuit voltages – a comparative study, ACS applied materials & interfaces 1 (2009) 2768–2777.
[24] F.C. Krebs, K. Norrman, Using light induced thermocleavage in a roll-to-roll process for polymer solar cells, ACS applied materials & interfaces 2 (2010) 877–887.